Title

JCAD Promotes Progression of Nonalcoholic Steatohepatitis to Liver Cancer by Inhibiting LATS2 Kinase Activity

Journal

Cancer Research, 77(19)

ISSN

0008-5472 1538-7445

Authors

Ye, Juan
Li, Tian-Sheng
Xu, Gang
et al.

Publication Date

2017-10-01

DOI

10.1158/0008-5472.CAN-17-0229

Peer reviewed

Published OnlineFirst August 3, 2017; DOI: 10.1158/0008-5472.CAN-17-0229

Molecular and Cellular Pathobiology

Cancer Research

JCAD Promotes Progression of Nonalcoholic Steatohepatitis to Liver Cancer by Inhibiting LATS2 Kinase Activity

Juan Ye[1], Tian-Sheng Li[1], Gang Xu[1], Yi-Ming Zhao[2,3], Ning-Ping Zhang[2], Jia Fan[2,4], and Jian Wu[1,2]

Abstract

Nonalcoholic steatohepatitis-associated hepatocellular carcinoma (NASH-HCC) is a malignancy whose incidents are rapidly increasing. However, the mechanisms that drive development of HCC in a steatotic microenvironment remain unknown. Here we report that the obesity-associated protein JCAD is expressed at significantly higher levels in human NASH-HCC specimens compared with pericarcinoma specimens. High JCAD expression was verified in multiple hepatoma cell lines. Forced overexpression of JCAD in hepatoma cells promoted tumor growth and proliferation, whereas JCAD silencing yielded opposite effects. JCAD interacted with the kinase domain of the tumor suppressor kinase LATS2, a core component of the Hippo signaling pathway. JCAD overexpression inhibited the ability of LATS2 to phosphorylate YAP in this pathway, in turn upregulating CCND1 and GLI2 to promote hepatoma cell proliferation. JCAD was induced by fatty acid overload in hepatic cells and was highly expressed in a mouse model of NASH-precarcinoma lesions, where the ratio of phospho-YAP to YAP was decreased. In human NASH-HCC specimens, JCAD expression and YAP phosphorylation patterns paralleled with the mouse model. Our findings illuminate a new role for JCAD and its critical interplay in the Hippo signaling cascade during the transition of NASH to HCC, with potential implications for therapeutic development in this setting. *Cancer Res; 77(19); 5287–300. ©2017 AACR.*

Introduction

Nonalcoholic fatty liver disease (NAFLD) includes a wide spectrum of disorders with fat accumulation, from simple fatty liver (SFL), a progressive form of nonalcoholic steatohepatitis (NASH), and fibrosis/cirrhosis to NASH-associated hepatocellular carcinoma (NASH-HCC; ref. 1). In the last few decades, NAFLD has emerged as the major cause of chronic liver disease in most parts of the western world (2), and approximately 1.0 billion individuals are affected worldwide, ranging from 10% to 36% of the general population (1, 3). As a liver-associated complication of diabetes, metabolic syndrome, and obesity, NASH requires medical attention, progresses to end-stage liver disease (ESLD or cirrhosis), and is currently the second leading etiology of liver disease in patients awaiting liver transplantation in the United States (4). NASH-HCC has become the major factor contributing to an increased HCC incidence in the United States (5–7). The multifactorial features of NASH and its progression determine the pathogenic complexity of HCC development in a steatotic microenvironment. Tremendous efforts have already been put into this field to elucidate the role of adaptive immunity through $CD8^+$ and NKT cells in the development of NASH-HCC in mice fed a high-fat/choline-deficient diet with a series of knockout manipulations (8). The crucial role of innate immunity in NASH-HCC development was supported by a recent study that demonstrated that the suppression of Th17 cell differentiation or blocking IL17A signaling prevents NASH and subsequent HCC development (9). Moreover, an elegant study emphasized the importance of gut microbiota in NASH progression and noted that senescent hepatic stellate cells (HSC) may be critical for the transformation of steatotic hepatocytes to malignant cells (10). Growing evidence in laboratory studies has narrowed the gap in our understanding of oncogenic processes that occur through genetic and epigenetic control, cellular interactions, and molecular signaling (11). However, currently available information does not clearly provide a complete understanding of molecular interplays that occur during NASH progression and hepatic carcinogenesis. Both basic and clinical investigations of NASH-HCC have not been able to identify molecular targets for therapeutic intervention or biomarker use, nor have they established guidelines for monitoring the transformation process.

To investigate the progression of NASH to HCC, we established a differential gene expression profile by analyzing significant expression changes in pathologically confirmed NASH-HCC and pericarcinoma specimens using Affymetrix microarrays. An obesity-associated gene, *KIAA1462*, was selected from the highly

[1]Department of Medical Microbiology, Key Laboratory of Molecular Virology, School of Basic Medical Sciences, Fudan University, Shanghai, China. [2]Shanghai Institute of Liver Diseases, Fudan University Shanghai Medical College, Shanghai, China. [3]Fudan University Shanghai Cancer Center, Shanghai, China. [4]Institute of Liver Cancer, Zhongshan Hospital, Fudan University, Shanghai, China.

Note: Supplementary data for this article are available at Cancer Research Online (http://cancerres.aacrjournals.org/).

J. Ye and T. Li contributed equally to this article.

Corresponding Authors: Jian Wu, Department of Medical Microbiology, Key Laboratory of Molecular Virology, Fudan University School of Basic Medical Sciences, 138 Yixue Yuan Road, P.O. Box 228, Shanghai 200032, China. Phone: 8621-5423-7705; Fax: 8621-6422-7201; E-mail: jian.wu@fudan.edu.cn; and Jia Fan, Liver Cancer Institute, Fudan University-Affiliated Zhongshan Hospital, 180 Fengling Road, Shanghai 200032, China. Phone: 86-21-6443-9027; Fax: 86-21-6403-7269; E-mail: fan.jia@zs-hospital.sh.cn.

doi: 10.1158/0008-5472.CAN-17-0229

Published OnlineFirst August 3, 2017; DOI: 10.1158/0008-5472.CAN-17-0229

expressed genes in NASH-HCC tissues. The nucleotide sequence of *KIAA1462* encodes for 1390 amino acids (aa), and no functional domains have been characterized in this protein. Recently, *KIAA1462* was identified as a molecular component of endothelial cadherin (E-cadherin)-based cell–cell junctions (12). Moreover, as a junction protein, the protein of *KIAA1462* is associated with coronary artery disease (13, 14). Hence, the protein of *KIAA1462* is named as junctional protein-associated with coronary artery disease (JCAD). The JCAD sequence is highly conserved in vertebrates from zebrafish to human (12), which indicates that the protein may have an important biological function. JCAD has been recently thought to be a novel candidate gene for a pathogenic role in serous borderline tumorigenesis (15). To our knowledge, its participation in oncogenesis has not been explored yet, nor has the role of JCAD in hepatic pathophysiology and carcinogenesis been investigated.

In the current study, we examined the role of JCAD in modulating tumorigenesis by manipulating its expression levels in hepatoma cells, determining its interaction with large tumor suppressor kinase 2 (LATS2), and inhibiting its kinase activity to influence HCC cell proliferation. Moreover, we employed a mouse model of NASH-precarcinoma lesions and human NASH-HCC specimens to verify findings from other systems. Our findings suggest that JCAD may have potential to serve as a valued biomarker in the progression of NASH to HCC and may facilitate the development of targeting therapeutics in improving the outcome of NASH-HCC treatment.

Materials and Methods

Human NASH-HCC specimens

Paraffin-embedded paired tumor and pericarcinoma tissues ($n = 12$) were obtained from the Biorepository of Fudan University Institute of Liver Cancer. Only four pairs of specimens with sufficient RNA quantity and quality were used for the Affymetrix microarray analysis, and the remaining RNA was enough to detect JCAD expression by qRT-PCR. Ten pairs of additional NASH-HCC frozen specimens were obtained in the same way and were stored at −80°C immediately after resection. All patients who underwent surgical resection were diagnosed with NASH-HCC without HBV or HCV infection and alcoholic liver disease, and provided written informed consent for the use of tissue specimens in medical research when the specimens were collected in the biorepository. The use of human tissue was approved by the Ethic Committee of Fudan University School of Basic Medical Sciences, and followed guidelines of the Helsinki Declaration and the national, municipal, and university regulations.

Animals

Male mice of C57BL/6J strain (8–12 weeks of age) were purchased from Nanjing University Institute of Animal Models (Nanjing, China), used to establish model of NASH-precarcinoma lesions. Male BALB/c nude mice (4–5 weeks of age) from Slack Company were used to establish a subcutaneous xenograft tumor model. All mice were housed in a specific pathogen-free facility with 12-hour light/dark cycle at 21–23°C. All animal experimental protocols were approved by the Animal Ethic Committee of Fudan University School of Basic Medical Sciences, and performed in the line with NIH Guidelines for Experimental Animal Handling and Use, as well as the national, municipal, and university regulations.

Cell culture

Huh-7 cell line was kindly provided by Professor Mark Feitelson, PhD from Temple University (Philadelphia, PA) in 2005. Huh-7-Trans cell line was isolated from Huh-7 cell line in 2014, as we reported previously (16). HLE and HLF cells were obtained from the Health Science Research Resources Bank in 2003. SK-Hep1, HepG2 and Hep3B cells were obtained from the ATCC in 2003. L02, SMCC-7721, MHCC-97H, and MHCC-97L were obtained from the Institute of Liver Cancer, Fudan University-Affiliated Zhongshan Hospital (Shanghai, China) in 2014. All cell lines in our laboratory were passaged no more than 30 passages after resuscitation, and were routinely tested for Mycoplasma contamination using PCR. Except Hep3B, HepG2, and SK-Hep1, remaining cell lines were incubated in DMEM supplemented with 10% (v/v) FBS, 1% (v/v) penicillin/streptomycin, 1% (v/v) L-glutamine and 1% (v/v) sodium pyruvate. Hep3B and HepG2 cells were incubated in minimum essential medium (MEM) supplemented with 10% (v/v) FBS, 1% (v/v) penicillin/streptomycin, 1% (v/v) L-glutamine, and 1% (v/v) sodium pyruvate (all from Life Technologies). All cell lines were cultured in a humidified incubator at 37°C with 5% CO_2 in air.

Cell proliferation assay

A water-soluble tetrazolium salt (WST-1) reagent (Sigma Aldrich) was used to determine the proliferation rate of different cells. Five thousand cells in 100 μL of medium were plated in each well of a 96-well plate and incubated overnight. The next day, 10 μL WST-1 reagent was added. After a further incubation of 4 hours, optical density (OD) was measured spectrophotometrically at a wavelength of 450 nm, and the background was corrected at 650 nm. At least three experiments were repeated independently in triplicate.

The YAP phosphorylation assay in JCAD-transfected cells

To determine the effect of JCAD on LATS2-mediated YAP phosphorylation at Ser127, 293T cells were seeded into 6-well plates and transfected in combination of HA-YAP with HA-MST2 (MST2 is an activator of LATS2, and it acts as a positive control), HA-JCAD or a control vector by Lipofectamine 2000 (Thermo Fisher Scientific) according to a previous report with some modifications (17). Thirty-six hours after transfection, cells were lysed in lysis buffer (25 mmol/L Tris, 150 mmol/L NaCl, 1 mmol/L EDTA, 1% NP40, 5% glycerol; pH 7.4) containing 1× protease inhibitor cocktail and 1× phosphatase inhibitor cocktail. The lysates were centrifuged at 12,000 × *g* for 10 minutes at 4°C. After measured protein concentration by a bicinchoninic acid assay (BCA) kit (Thermo Fisher Scientific), 30 μg of protein lysate was mixed with 5× SDS sample buffer, boiled for 10 minutes at 100°C, and subjected to electrophoresis.

Kinase assays

To further detect the effect of JCAD on LATS2 kinase activity, 293T cells seeded in 6-well plates were transfected with a combination of Myc-LATS2 and HA-MST2, HA-JCAD or a control vector using Lipofectamine 2000 (18). Thirty-six hours after transfection, cells were lysed in immunoprecipitation buffer (25 mmol/L Tris, 150 mmol/L NaCl, 1 mmol/L EDTA, 1% NP40, 5% glycerol, pH 7.4), and the immunoprecipitated LATS2 was captured by Myc-tag magnetic beads. The immunoprecipitated LATS2 protein was subjected to a kinase assay in 30 μL of kinase assay buffer containing 25 mmol/L Tris-HCl, pH 7.4; 1 mmol/L

Published OnlineFirst August 3, 2017; DOI: 10.1158/0008-5472.CAN-17-0229

DTT; 10 mmol/L MgCl2; and 1 × protease inhibitor, supplemented with 500 μmol/L ATP (AMRESCO) and 1 μg of His-YAP expressed in *Escherichia coli* as the substrate. The reaction mixture was incubated at 30°C for 30 minutes, stopped by addition of 5× SDS loading buffer, boiled for 10 minutes at 100°C, and subjected to Western blot analysis for the detection of p-YAP.

Xenograft growth in nude mice

To detect tumor growth *in vivo*, a total of 2.5×10^6 Huh-7 (JCAD-KD and control) and 3.0×10^6 SMCC-7721 (JCAD-OE and control) cells were inoculated into franks of nude mice subcutaneously, respectively. Tumor volume and body weight were measured every five days after inoculation. Mice bearing xenografts were humanely sacrificed in accordance with guidelines approved by the Animal Ethic Committee of Fudan University School of Basic Medical Sciences 20–25 days after the inoculation for further analysis.

Animal model of NASH-precarcinoma lesions induced by a high-fat/calorie diet plus high fructose and glucose

C57BL/6J mice were fed a high-fat/calorie (HFC) diet *ad libitum* with the consumption of high levels of fructose and glucose (23.1 g/L D-fructose plus 18.9 g/L D-glucose) in drinking water for 12 months, as described previously (2). The diet was obtained from RESEARCH DIET, with 60% kcal from fat and containing 0.1% cholesterol. Mice fed a regular chow diet were used as controls. The mice were humanely sacrificed after 5, 9, and 12 months of feeding, and liver specimens were collected for histopathologic analysis and determination of JCAD expression and p-YAP/YAP ratio.

Statistical analysis

All experiments were repeated at least for three times independently and the results were expressed as means ± SEM. Statistical analysis was performed using SPSS program version 17.0. Normal distribution was performed in all data. Numerical data in a normal distribution between two groups were analyzed by a variance test of homogeneity, then by Student *t* test. Data between two groups that do not stay in a normal distribution were analyzed by nonparametric Mann–Whitney *U* test. *P* value less than 0.05 was considered to be statistically significant.

Results

JCAD was highly expressed in NASH-HCC specimens

To investigate the differentially expressed genes in NASH-HCC specimens, we established a gene expression profile from four sets of NASH-HCC and pericarcinoma specimens using Affymetrix microarrays. Functional analysis (GO enrichment) of the differentially expressed genes indicated that they are involved in protein binding, cell migration, differentiation and adhesion, as well as junction anchoring (Fig. 1A). Then we observed a striking difference in expression of 26 genes (12 downregulated and 14 upregulated) concerning inflammation, oncogenesis, and angiogenesis between NASH-HCC and pericarcinoma tissues (Fig. 1B). The most differentially expressed genes included those that were downregulated, such as CNOT6L (cell proliferation, decreased by 90%) and CLEC4M (immune surveillance, decreased by 80%), and those that were upregulated, such as JCAD (adhesion junction, increased up to 6-fold), CD36 (angiogenesis, inflammatory response, fatty acid metabolism, increased up to 7-fold), and ZMYND11 (transcriptional repression and activation, increased up to 10-fold; Fig. 1C).

JCAD promoted hepatoma cell proliferation and increased colony formation and spheroid formation *in vitro*

Quantitative RT-PCR verified that JCAD was highly expressed in NASH-HCC compared with pericarcinoma tissues in an increased number of NASH-HCC specimens, as shown in Fig. 2A. We further confirmed JCAD expression in 10 hepatoma cell lines using immortalized hepatocellular L02 cells as a control by a quantitative RT-PCR assay. JCAD was highly expressed in many hepatoma cell lines, especially in Huh-7 (42-fold), Huh-7-Trans (13-fold), HLE (10-fold) and HLF (6-fold) cells, whereas a relatively low expression level was seen in SMCC-7721 (1.3-fold) and SK-Hep1 (2-fold) cells compared with L02 cell line (Fig. 2B and C).

To further investigate the biological function of JCAD in hepatoma cells, we inhibited basal expression of JCAD in Huh-7-Trans, Huh-7, HLE, and HLF cells or overexpressed JCAD in SMCC-7721 cell. qRT-PCR and Western blot results confirmed the successful knockdown by an RNAi approach (approximately 70%–80% decrease) or overexpression of JCAD (approximately 60-fold increase) by lentiviral transduction with the full sequence of JCAD in these cell lines (Fig. 2D and E; $P < 0.05$).

To investigate the tumorigenic role of JCAD in hepatoma cells with JCAD-KD or JCAD-OE, a WST-1 assay was used to examine the effect of JCAD on proliferation of hepatoma cells. The proliferation of hepatoma cells with JCAD-KD was markedly suppressed in comparison with the control cells, except for HLF cells, probably due to a lower basal JCAD expression in HLF cells than in Huh-7 and Huh-7-Trans cells. In contrast, proliferation of hepatoma cells with JCAD-OE was strikingly enhanced compared with that of the control cells (Fig. 2F; $P < 0.05$).

To further confirm the role of JCAD in tumorigenesis *in vitro*, we performed a colony formation experiment with stable JCAD-KD or JCAD-OE cells and corresponding control cells. The colony formation of hepatoma cells with JCAD-KD was much lower than that of control cells (down by 60%–70%), whereas JCAD overexpression markedly enhanced colony formation (enhanced up to approximately 2-fold; Fig. 2G; $P < 0.05$). Moreover, spheroid formation was used to further verify tumor formation potential (Fig. 2H). The spheroid formation of hepatoma cells (Huh-7-Trans, Huh-7) with JCAD-KD was much lower than that of cells transfected with a control lentivirus; whereas JCAD-overexpressing cells (SMCC-7721) exhibited enhanced capability of spheroid formation ($P < 0.05$). However, as shown in Fig. 2H, there was no significant difference between HLE-KD cells or HLF-KD cells and their control cells, which may be due to a lower basal JCAD expression in HLE and HLF cells compared with that in Huh-7 and Huh-7-Trans cells. In summary, our data demonstrated that JCAD promotes the proliferation and tumor formation *in vitro*.

JCAD promoted xenograft growth *in vivo*

To further investigate whether JCAD might regulate hepatoma xenograft growth *in vivo*, Huh-7 with stable JCAD-KD and SMCC-7721 with JCAD-OE and their corresponding control cells were subcutaneously injected into athymic nude mice, respectively. JCAD silence resulted in an approximate 40% reduction in weight and 20% reduction in size of xenograft tumors compared with those of control xenografts (Fig. 3A and B; $P < 0.05$). The xenograft tumors derived from JCAD-KD cells appeared to be

Published OnlineFirst August 3, 2017; DOI: 10.1158/0008-5472.CAN-17-0229

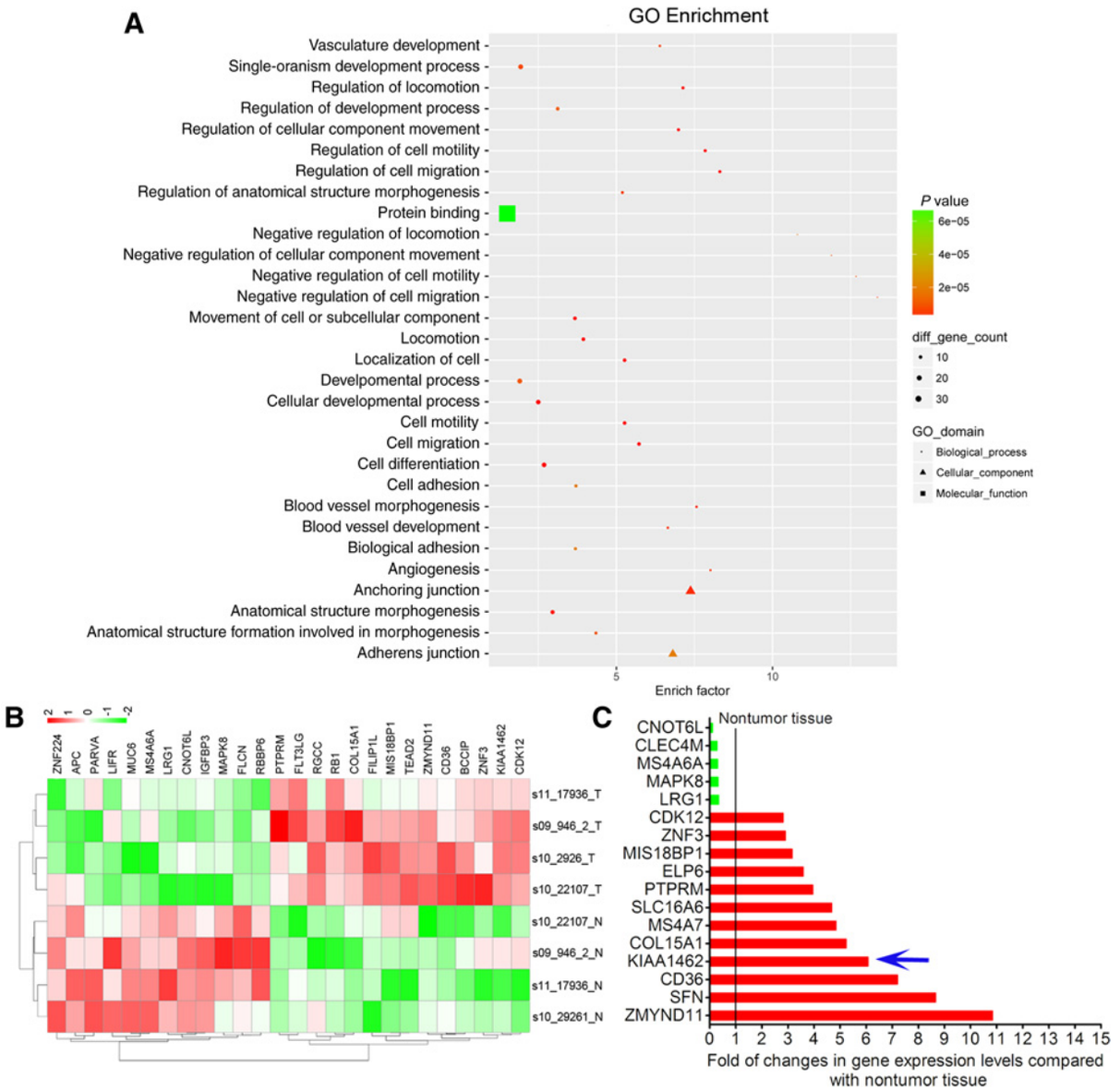

Figure 1.

JCAD was highly expressed in NASH-HCC specimens. **A,** GO enrichment analysis of the differentially expressed genes in NASH-HCC and pericarcinoma tissues. Color indicates the fold change, and expression level increases from blue to orange, as indicated in the scale bar. Dots, triangles, and squares represent biological processes, cellular components, and molecular function, respectively, whereas the size of the shape indicates the number of genes. **B,** Differential expression of significant genes (including upregulated and downregulated genes) from NASH-HCC specimens is shown in a heatmap. The red color represents enhanced expression, whereas the green represents decreased expression, as indicated in the scale bar. **C,** Fold changes in gene expression levels compared with those in paired pericarcinoma liver tissue. The red color represents genes with upregulated expression, whereas the green represents genes with downregulated expression.

morphologically different from control cell–derived tumors, as determined by a histologic analysis (Fig. 3C), indicating that JCAD-KD could repress tumorigenesis. qRT-PCR and Western blot analyses confirmed the persistent reduction in JCAD expression levels in xenograft tumors (Fig. 3D and E; $P < 0.05$). Mice injected with JCAD-overexpressing cells exhibited a 2-fold increase in the weight and 3-fold increase in size of xenograft tumors compared with those of control xenografts (Fig. 3F and G; $P < 0.05$). Histologically, tumors derived from JCAD-OE cells appeared to have a higher cell density, as reflected by more nuclei in xenografts, than those derived from control cells (Fig. 3H), indicating that JCAD-OE could enhance tumorigenesis. qRT-PCR and Western blot analyses confirmed an increase in JCAD levels in dissected xenograft tumors compared with that in control xenografts (Fig. 3I and J; $P < 0.05$). The extent of reduction or increase in HCC xenograft growth was consistent with the growth rate of hepatoma cells with JCAD knockdown or overexpression observed *in vitro*. Altogether, these results indicate that JCAD is involved in hepatoma cell growth *in vitro* and *in vivo*, further confirming its prooncogenic function in hepatoma cells.

Published OnlineFirst August 3, 2017; DOI: 10.1158/0008-5472.CAN-17-0229

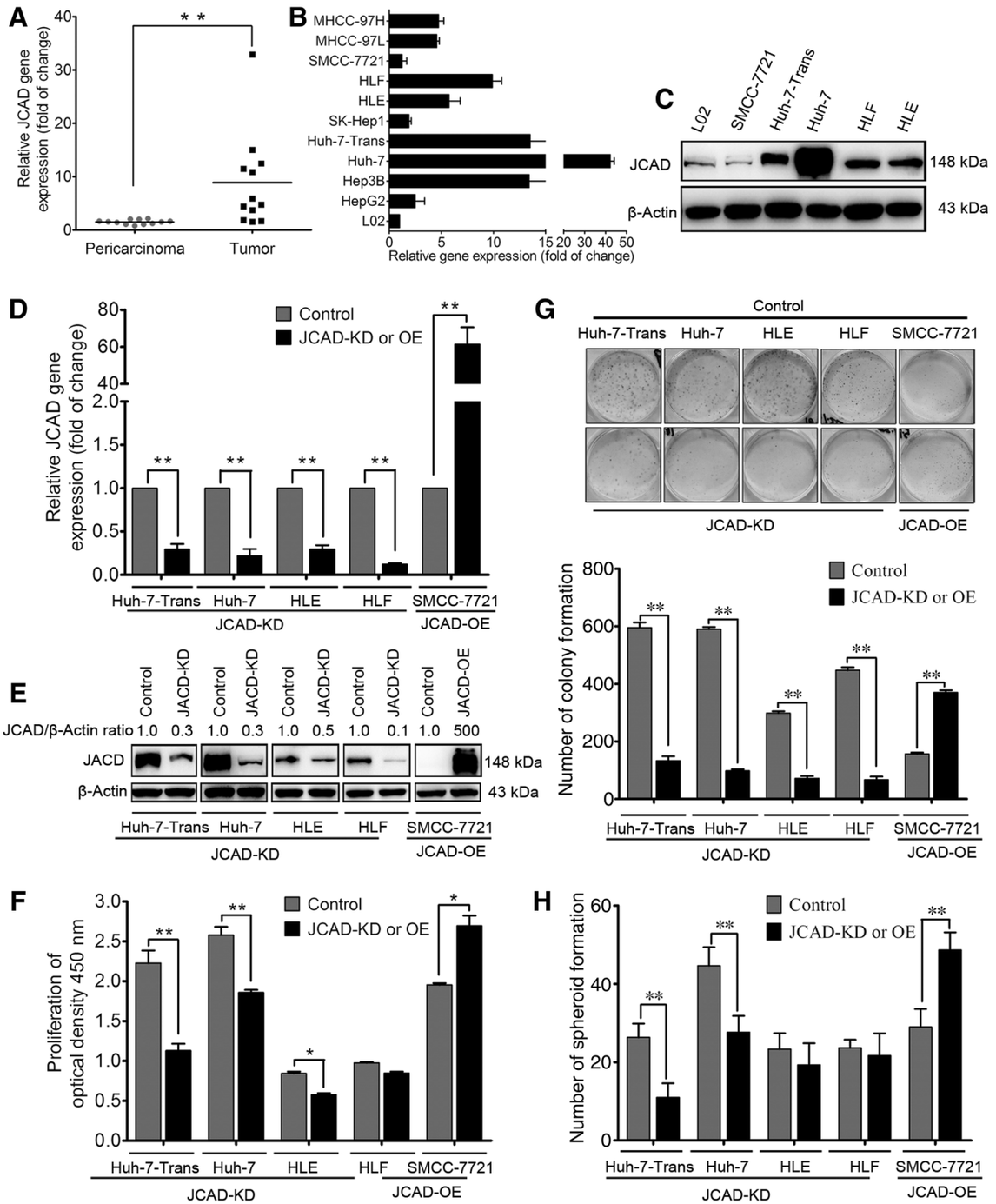

Figure 2.

JCAD promoted hepatoma cell proliferation, and increased colony formation and spheroid formation *in vitro*. **A,** JCAD mRNA levels in NASH-HCC human specimens compared with pericarcinoma by quantitative RT-PCR analysis ($n = 12$ per group). **B,** JCAD mRNA levels in hepatoma cells compared with L02 cell line by quantitative RT-PCR analysis. **C,** Relative JCAD protein amount in hepatoma cells was examined by Western blot analysis. **D,** qRT-PCR analysis of JCAD mRNA levels in stable JCAD-KD (Huh-7, Huh-7-Trans, HLE, and HLF), stable JCAD-OE (SMCC-7721), and control cells. The *y*-axis represents the ratio of JCAD over GAPDH expression, with the control set to 1.0. **E,** Western blot analysis of JCAD protein levels in stable JCAD-KD (Huh-7, Huh-7-Trans, HLE, and HLF), stable JCAD-OE (SMCC-7721), and control cells. β-Actin was used as a loading control. The densitometrical ratio of JCAD over β-actin is shown with the control set to 1.0. **F,** Proliferation of stable JCAD-KD (Huh-7, Huh-7-Trans, HLE, and HLF), stable JCAD-OE (SMCC-7721), and control cells determined by WST-1 assay. **G,** Representative images and the quantification of colony formation in stable JCAD-KD (Huh-7, Huh-7-Trans, HLE, and HLF) cells, stable JCAD-OE (SMCC-7721), and control cells. The quantification of colony formation is in the panel below that. The *y*-axis represents the colony number. **H,** Quantification of spheroid formation in stable JCAD-KD (Huh-7, Huh-7-Trans, HLE, and HLF) cells, stable JCAD-OE (SMCC-7721), and control cells. The *y*-axis represents the spheroid formation number. *, $P < 0.05$; **, $P < 0.01$ compared with the control.

Published OnlineFirst August 3, 2017; DOI: 10.1158/0008-5472.CAN-17-0229

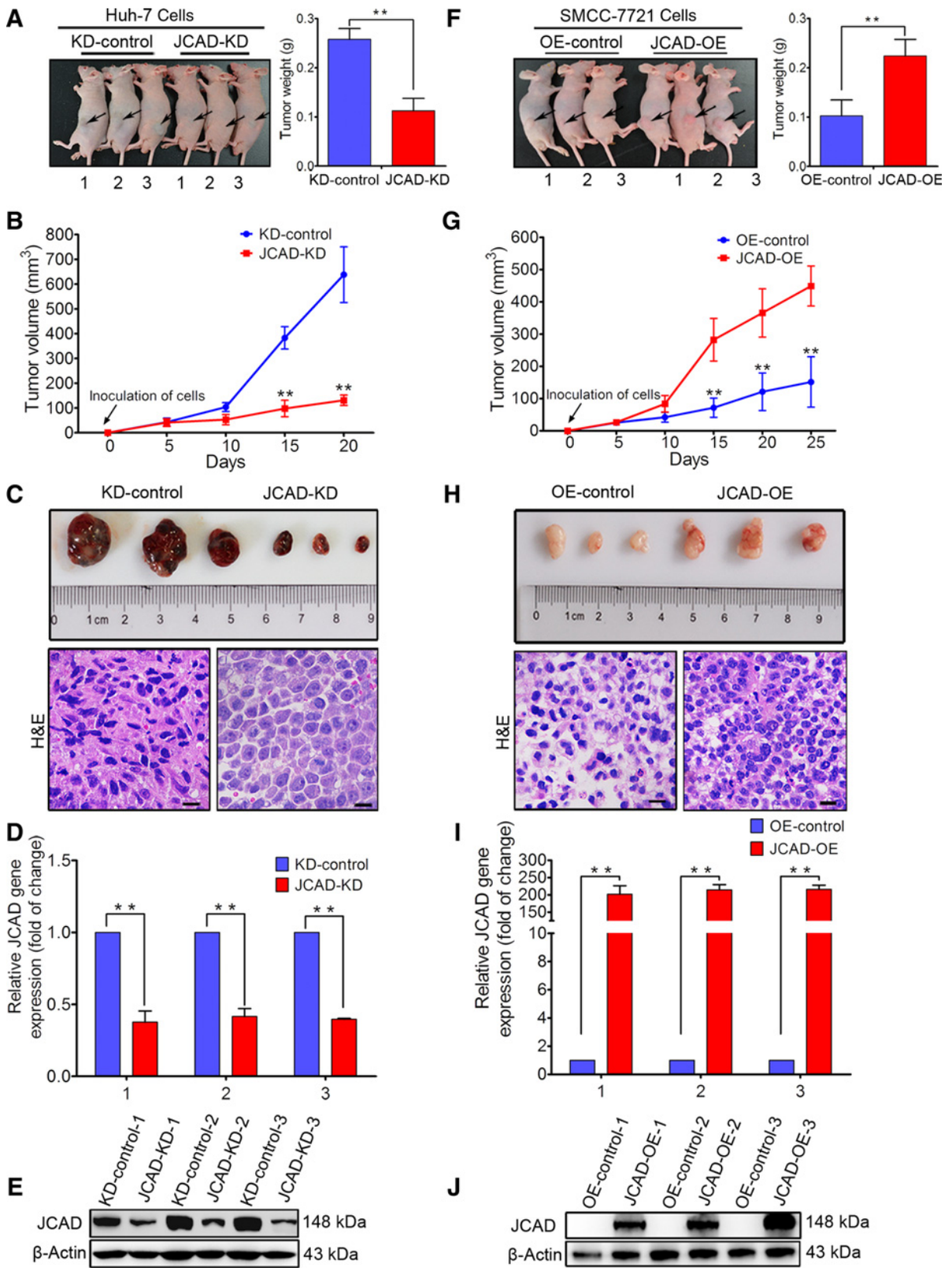

Published OnlineFirst August 3, 2017; DOI: 10.1158/0008-5472.CAN-17-0229

JCAD inhibited kinase activity of LATS2 by binding to its kinase domain

To reveal the physiologic function of JCAD, we firstly investigated the colocalization of JCAD with LATS2, which is a negative regulator of YAP in the Hippo signaling pathway that plays a pivotal role in organ size control and tumor growth. Immunofluorescent staining revealed that JCAD was colocalized with LATS2 in proximity to the nuclear membrane in 293T and Huh-7 cells (Fig. 4A). We performed a coimmunoprecipitation assay by overexpressing HA-JCAD and Myc-LATS2 in 293T cells or overexpressing Myc-LATS2 in Huh-7-Trans and Huh-7 cells (both of which overexpressed JCAD), and then analyzed the isolated protein complexes by Western blot analysis using a JCAD antibody. The results documented that JCAD interacts with LATS2 in 293T, Huh-7-Trans, and Huh-7 cells, as indicated by the arrow (Fig. 4B). MOB is another important regulator of the Hippo signaling pathway, and interacts with LATS2 to promote its activation. We also examined whether JCAD affects LATS2 interaction with MOB. As shown in Supplementary Fig. S1A, JCAD did not affect the interaction of LATS2 with MOB. In addition, it seemed that JCAD did not interact directly with MOB neither (the data not shown). There are four functional domains of LATS2 based on its peptide sequence (Fig. 4C). To determine which domain of LATS2 interacts with JCAD, we constructed different constructs with multiple deletion mutations in LATS2 domains (17). As indicated by the arrow in Fig. 4D, a coimmunoprecipitation assay with an HA-tag antibody verified that JCAD bound to the kinase domain of LATS2 (amino acids 668–974), which was predicted to be catalytically inactive and adjacent to the MOB1-binding region.

In the Hippo signaling pathway, LATS2 acts as a protein serine/threonine kinase that phosphorylates YAP to regulate downstream effects. We therefore examined whether the interaction of JCAD affects the kinase ability of LATS2, a His-tagged fusion protein His-YAP was expressed in *Escherichia coli* and purified as a substrate. We then measured the phosphorylation level of His-YAP by a p-YAP (s127) antibody. JCAD expression decreased LATS2 kinase activity, as demonstrated by the inhibition of YAP phosphorylation (shown by the arrow; Fig. 4E). Moreover, in JCAD-transfected cells, HA-JCAD markedly suppressed YAP phosphorylation compared with those transfected with a control plasmid and a positive control plasmid HA-MST2, as indicated by the arrow (Fig. 4F). In this assay, HA-MST2 was used as a positive control to activate LATS2 kinase activity of the phosphorylation on YAP.

JCAD induced dephosphorylation and nuclear localization of YAP

To investigate the JCAD effect on the ability of LATS2 to phosphorylate YAP and further determine whether JCAD acts as a regulator in the Hippo signaling pathway to regulate hepatoma cell proliferation, we examined the expression levels of LATS2, CCND1, GLI-2, p-YAP, and YAP in JCAD-KD and JCAD-OE cells. As shown in Fig. 5A and B, p-YAP was upregulated in JCAD-KD cells and downregulated in JCAD-OE cells, whereas LATS2 and YAP did not significantly change. JCAD only affected kinase activity of LATS2 by interacting with the kinase domain, but not altering its expression. TAZ is another important regulator that has a function similar to YAP in the Hippo signaling pathway. Hence, we determined expression levels of TAZ and p-TAZ in JCAD-KD and JCAD-OE cells. As shown in Supplementary Fig. S1B, JCAD did not affect expression levels of both TAZ and p-TAZ. Moreover, expression levels of downstream genes, *CCND1* (decreased by 60%) and *GLI-2* (decreased by 30%), were downregulated in hepatoma cells with JCAD-KD compared with control cells ($P < 0.05$); meanwhile, the levels of CCND1 (increased up to 1.5-fold) and GLI-2 (increased up to 1.6-fold) were upregulated in hepatoma cells with JCAD-OE compared with control cells ($P < 0.05$). To exclude possible off-targeting effects of JCAD shRNA silencing, the functional recovery by reexpressing JCAD with the modified cDNA was performed in JCAD-KD cells (Huh-7-Trans, HLE, and HLF; Supplementary Fig. S2A). As shown in Supplementary Fig. S2B and S2C, JCAD was reexpressed in JCAD stable knockdown cells. Proliferation was restored in JCAD reexpressed cells as indicated by WST-1 assay shown in Supplementary Fig. S2D. Moreover, expression level of p-YAP was downregulated accordingly in JCAD reexpressed cells (Supplementary Fig. S2E); meanwhile, the downstream genes (CCND1 and GLI-2) of the Hippo signaling pathway were upregulated. This recovery assay further confirmed that the reduction of JCAD expression was specifically responsible for decreased cell proliferation in JCAD-KD cells. The altered expression of YAP target genes (*CCND1* and *GLI-2*) in combination with the results of the above recovery experiment indicate that JCAD may indeed act as a novel upstream regulator of the Hippo signaling pathway to affect hepatoma cell proliferation.

YAP is transcriptionally active when it is translocated into the nucleus (19). The dephosphorylation of YAP promotes YAP nuclear translocation and upregulates the YAP/TEAD association, leading to YAP/TEAD transcriptional activation, and activates target gene (GLI2 and CCND1) expression (20, 21). Therefore, we addressed whether JCAD affected YAP nuclear translocation. In Huh-7 and Huh-7-Trans control cells, endogenous YAP was localized in the nucleus (Fig. 5C). However, JCAD knockdown caused a dramatic redistribution of YAP from the nucleus to the cytoplasm (Fig. 5C) as showed with arrows, especially in Huh-7 cells. In contrast, JCAD overexpression increased YAP nuclear translocation, although not so dramatically. This was confirmed by Western blot analysis with cytosolic and nuclear fraction protein extracts. As shown in Supplementary Fig. S3, knockdown of JCAD reduced the level of nuclear YAP; at the same time, remarkably increased the relative level of YAP phosphorylation in the cytosolic compartment in Huh-7 cells. These results suggest that JCAD may cause YAP nuclear translocation through phosphorylation by LATS2.

Figure 3.

JCAD promoted xenograft growth *in vivo*. **A** and **F,** JCAD-KD cells (Huh-7), JCAD-OE cells (SMCC-7721), and control cells were injected subcutaneously into the flank areas of nude mice, respectively. Representative images and weight of xenograft tumors derived from JCAD-KD or JCAD-OE and control cells ($n = 3$ per group). **B** and **G,** Quantification of tumor volume ($n = 3$ per group), showing that JCAD silencing reduced tumor growth, while JCAD overexpression promoted tumor growth. **C** and **H,** Representative images of tumor size and hematoxylin and eosin (H&E) images (magnification, × 40; scale bars, 10 μm) of tumors derived from JCAD-KD, JCAD-OE, and control cells, as indicated ($n = 3$ per group). **D** and **I,** qPCR analysis of JCAD expression in xenograft tumors derived from JCAD-KD, JCAD-OE, and control cells. The *y*-axis represents the ratio of JCAD over GAPDH expression, with the control set to 1.0. **E** and **J,** Western blot analysis of JCAD protein levels in xenograft tumors derived from JCAD-KD, JCAD-OE, and control cells. β-Actin was used as a loading control. *, $P < 0.05$; **, $P < 0.01$ compared with the control.

Published OnlineFirst August 3, 2017; DOI: 10.1158/0008-5472.CAN-17-0229

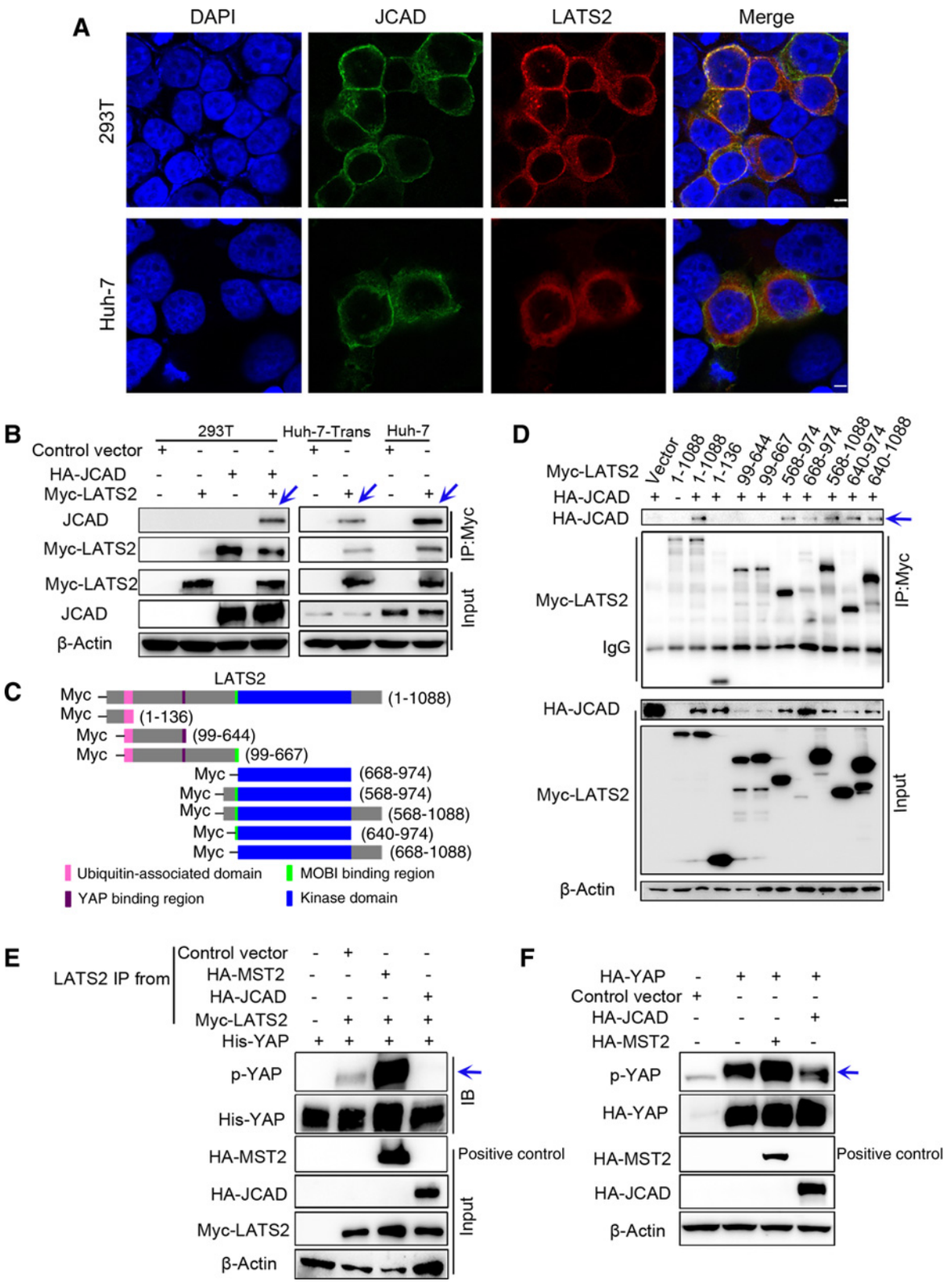

Published OnlineFirst August 3, 2017; DOI: 10.1158/0008-5472.CAN-17-0229

JCAD was induced in hepatic cells with free fatty acid overload

As mentioned above, JCAD is associated with obesity and highly expressed in NASH-HCC specimens. To determine whether fatty acid overload affects JCAD expression, we treated immortalized L02 hepatocytes, Huh-7, and HepG2 hepatoma cells by free fatty acid (FFA) overload. Oil Red O staining confirmed lipid droplet accumulation after FFA overload (Fig. 6A). JCAD was highly expressed in these FFA-overloaded cells at both mRNA and protein levels compared with the control cells ($P < 0.05$; Fig. 6B and C), although how JCAD influences lipid metabolism is unknown. Together, these results indicate that JCAD could be induced in hepatic cells with free fatty overload.

JCAD was increased and the ratio of p-YAP over YAP was decreased in a mouse model of NASH-precarcinoma and NASH-HCC human specimens

We next examined JCAD expression in a mouse model of NASH-precarcinoma lesions and human specimens. First, liver histology and Oil Red O staining in frozen sections from mice fed a high-fat diet plus high fructose and glucose in drinking water for 5, 9, and 12 months indicated steatohepatitis, severe fibrosis, and dysplasia in hyperplastic nodules (other indicators confirmed by a separate investigation; Fig. 7A; ref. 22). As shown in Fig. 7B, JCAD expression was upregulated throughout the entire feeding period, while the ratio of p-YAP over YAP was downregulated. JCAD expression increased gradually with the severity of liver steatosis and fibrosis as well as the occurrence of dysplasia (1.9-fold increase at 5 months, 2.2-fold increase at 9 months, and 2.6-fold increase at 12 months), while the ratio of p-YAP over YAP decreased with NASH progression (60% decrease at 5 months, 40% decrease at 9 months, and 70% decrease at 12 months). Moreover, we performed qRT-PCR analysis to detect the core regulators of the Hippo signal pathway in the development of NASH-HCC animal models (5, 9, and 12 months). As shown in the Supplementary Fig. S4, expression levels of core regulators of Hippo signaling molecules, such as LATS2 and MST1/2 were lower ($P < 0.05$–0.01) along with the development of NASH-HCC; whereas, YAP, TAZ, and CCND1 appeared to be upregulated compared with the early stage (5 months). Therefore, these results further demonstrate that JCAD was highly upregulated during the transition from NASH to premalignant lesions of HCC and that other components of the Hippo signaling pathway were probably also involved in an intermediate stage of this transition in these animals.

To further determine whether JCAD overexpression occurs in human patients with NASH-HCC, we obtained additional ten pairs of human NASH-HCC and pericarcinoma specimens. JCAD expression was higher in five out of ten HCC specimens than that in the corresponding pericarcinoma tissue (Fig. 7C, sample no. 2, 5, 6, 8, and 9). Furthermore, the ratio of p-YAP over YAP was lower in these five sets of NASH-HCC specimens with higher JCAD expression as evaluated by Western blot analysis, although heterogeneity in expression of JCAD, YAP, and p-YAP was observed in different NASH-HCC specimens. Therefore, these results demonstrate that JCAD was highly upregulated in half of the analyzed human NASH-HCC specimens and may be involved in the development of NASH to HCC through the Hippo signaling pathway, although the exact mechanisms require further investigation and heterogeneity exists in terms of JCAD expression levels and involvement of the Hippo signaling pathway.

Discussion

NAFLD becomes one of the most common liver diseases in developed and developing countries and represents an increasing epidemic (23, 24). Its most active form, NASH, is believed to be a potential precursor of HCC (25). From limited clinical data, it appears that prognosis, risk factors and histopathologic features of NASH-associated HCC are obviously different from those secondary to other etiologies of liver disease, such as hepatitis B or C viral infection (1). Moreover, pathogenic factors contributing to the oncogenic process in a steatotic microenvironment are considered to differ from HBV or HCV infection, and have been largely undefined yet (26). Therefore, tremendous efforts are still demanded to understand hepatic carcinogenesis of NASH-HCC at the genetic, epigenetic, molecular, and cell levels in both laboratory and clinical settings.

In this study, we report a novel NASH-HCC candidate gene, *KIAA1462*, which encodes the JCAD protein identified as a molecular component of E-cadherin–based endothelial cell–cell junctions (12). As a junction protein, JCAD was shown to enhance tumor cell proliferation and growth in hepatoma cells and in nude mice in the current study (Figs. 2 and 3). Our finding also demonstrated that JCAD interacted with LATS2 (Fig. 4B), which is a core kinase component of the Hippo signaling pathway, encodes a Ser/Thr protein kinase and plays a critical role in mediating the progression of various malignant tumors, such as malignant mesothelioma and nasopharyngeal carcinoma (27–30). The Hippo signaling pathway consists of a core kinase cascade (MST1/2, MOB1/2 and LATS1/2) and controls organ size through the regulation of cell proliferation and apoptosis (31). When the Hippo signal pathway was activated, MOB1/2 interacts with and activates LATS2. Our findings indicated that JCAD directly interacted with LATS2 (Fig. 4B), and inhibited LATS2 to phosphorylate YAP to induce cell proliferation (Fig. 4E and F). We have found that JCAD did not affect the binding of MOB1/2 to LATS2 (Supplementary Fig. S1A), nor did it interact with MOB1/2 directly (data not shown). Up to date, we have not found the upstream regulators of JCAD. However, our preliminary results suggest that accumulation of fat acids in hepatic cells upregulated

Figure 4.

JCAD interacted with LATS2 and inhibited the ability of LATS2 to phosphorylate YAP. **A,** Representative confocal micrographs of the colocalization of JCAD (green) with LATS2 (red). DAPI (blue) was used for nuclear staining. Scale bars, 5 μm. The green and red color is overlaid in the proximity of the nucleus. **B,** Myc-LATS2 and HA-JCAD were individually or cotransfected into 293T cells; only Myc-LATS2 was transfected in Huh-7-Trans and Huh-7 cells (which highly expressed JCAD). Thirty-six hours after transfection, Myc-tag was immunoprecipitated, followed by Western blot analysis using JCAD antibodies as indicated by the arrows. The inputs are shown at the bottom. **C,** A schematic illustration of LATS2 deletion mutation constructs used in this study. **D,** Full-length HA-JCAD, Myc-LATS2, and deletion mutants were ectopically expressed, followed by Myc-tag-immunoprecipitations and Western blot analysis with HA (as indicated by an arrow) and Myc antibodies. IgG was used as a positive control. Inputs are shown in the bottom panel. **E,** Kinase activity assay was used to detect the effect of JCAD on LATS2. His-YAP was expressed in *Escherichia coli* and purified as a substrate. MST2 was used as a positive control to activate LATS2. The p-YAP level was determined by Western bolt analysis, indicated by an arrow. The protein levels of JCAD, LATS2, MST2, and β-actin are shown in the bottom panel. **F,** The relative levels of YAP, p-YAP, Myc-LATS2, Myc-JCAD, and β-actin were detected in cells cotransfected with HA-YAP and JCAD, LATS2, or a control vector. The level of p-YAP significantly decreased with JCAD cotransfection, as indicated by the arrow.

Published OnlineFirst August 3, 2017; DOI: 10.1158/0008-5472.CAN-17-0229

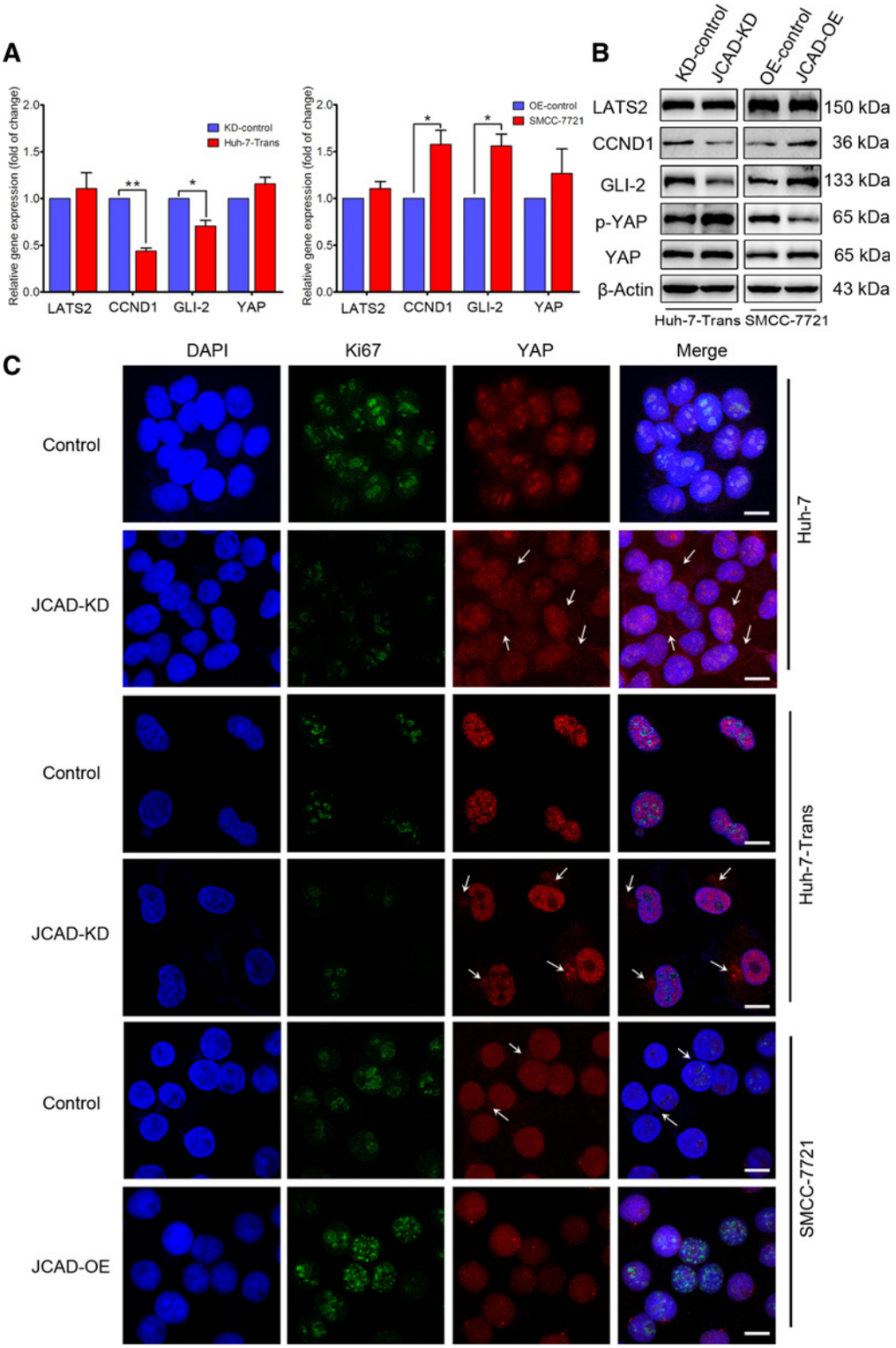

Figure 5.

JCAD acts as an upstream regulator of the Hippo pathway. **A,** qRT-PCR analysis of LATS2, CCND1, GLI-2, and YAP in stable JCAD-KD, stable JCAD-OE, and control cells. The *y*-axis represents the ratio of the gene of interest over GAPDH expression, with the control set to 1.0. *, $P < 0.05$; **, $P < 0.01$ compared with controls. **B,** Western blot analysis of LATS2, CCND1, GLI-2, p-YAP, and YAP levels in stable JCAD-KD, JCAD-OE, and control cells. **C,** Representative confocal micrographs of YAP (red) and Ki67 (green) in JCAD-KD (Huh-7 and Huh-7-Trans), JCAD-OE (SMCC-7721), and control cells. DAPI (blue) was used for nuclear staining. The translocation of YAP between cytoplasm and nucleus is indicated by white arrows. Scale bars, 25 μm.

Published OnlineFirst August 3, 2017; DOI: 10.1158/0008-5472.CAN-17-0229

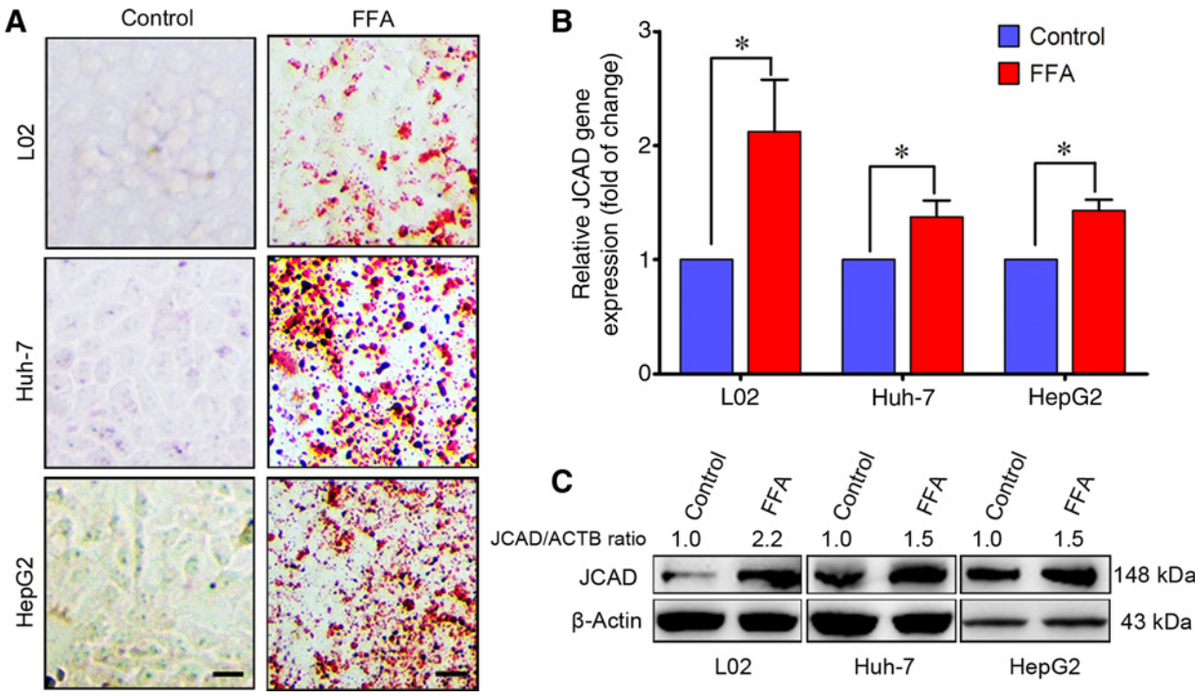

Figure 6.

JCAD was highly expressed in hepatic cells with fatty acid overload. **A,** Representative micrographs of Oil Red O staining in FFA-overloaded L02, Huh-7, and HepG2 cells (magnification, × 20). Scale bars, 10 μm. **B,** qRT-PCR analysis of JCAD expression in FFA-overloaded L02, Huh-7, and HepG2 and control cells. The *y*-axis represents the ratio of JCAD over GAPDH expression, with the control set to 1.0. *, $P < 0.05$; **, $P < 0.01$ compared with controls. **C,** Western blot analysis of JCAD protein levels in FFA-overloaded L02, Huh-7, and HepG2 and control cells. The densitometrical ratio of JCAD over β-actin is shown with the control set to 1.0. The data shown are from at least three independent experiments, with each in triplicates.

JCAD expression. Furthermore, JCAD binds to the kinase domain of LATS2 to reduce phosphorylation of YAP, which is a downstream effector and a transcriptional coactivator in the Hippo signaling pathway (32). The dephosphorylation of YAP promoted YAP nuclear translocation and upregulates the YAP/TEAD association, leading to YAP/TEAD transcriptional activation and proliferation in hepatoma cells (Fig. 7D; refs. 20, 21). TAZ exhibits a function similar to YAP; however, our findings showed that JCAD did not affect TAZ and its phosphorylation in JCAD-manipulated cells (Supplementary Fig. 1B). The phosphorylation is a critical step in the Hippo signaling process because phosphorylation of YAP prevents its translocation into the nucleus to activate downstream target genes (such as CCND1 and GLI-2), which are associated with cancer development, metastasis, and drug resistance as demonstrated in our previous studies (16, 33, 34). In this study, we confirmed that expression levels of CCND1 and GLI-2 were upregulated when JCAD was highly expressed. Taken together, our results indicate that JCAD may play an important role by interacting with LATS2 to prevent it from phosphorylating YAP, leading to CCND1 and GLI-2 upregulation and the promotion of HCC development.

The *KIAA1462* gene is located on chromosome HSA10p11.23, which harbors a major quantitative trait locus linked to or associated with morbid obesity (35–37). The protein of *KIAA1462*, JCAD was highly expressed in NASH-associated HCC specimens and its expression is inducible by fatty acid overload. Thereafter, we investigated JCAD expression during NASH progression in a mouse model of NASH-precarcinoma lesions (22). The sustained JCAD increase and the reduced p-YAP/YAP ratio in the livers of mice with NASH-precarcinoma lesions and in NASH-HCC specimens underscore the significance of the Hippo signaling pathway in NASH-HCC development, which has not been previously reported in the literature. Interestingly, the molecular weight of JCAD appeared to increase in mice with NASH progression (Fig. 7B). The exact mechanisms underlying this finding is unclear, however, our speculation is that as a phosphoprotein, JCAD may be posttranslationally phosphorylated at amino acid sites 1044, 1050, 1194, and 1281 in a steatotic environment. Given the limited availability of clinical specimens, the data from the current study did not allow us to correlate JCAD expression and YAP dephosphorylation with NASH-HCC histopathologic type, tumor size and number, aggressiveness, metastasis, and prognosis. Therefore, more investigations are warranted to explore the mechanism of progression from NASH to HCC.

To facilitate the understanding role of JCAD in the transition of NASH to HCC, an illustration is shown in Fig. 7D. In normal liver tissues, JCAD is maintained at a low level. When fatty acids are accumulated in the liver, high JCAD expression is induced. The excess JCAD markedly inhibits the ability of LATS2 to phosphorylate YAP. Phosphorylated YAP is retained in the cytoplasm, whereas unphosphorylated YAP is translocated into the nucleus to activate downstream genes, such as *GLI-2* and *CCND1*, which are morphogenic and proliferative to many cell types (33).

In conclusion, JCAD appears to be involved in the transition from NASH to HCC through the Hippo signaling pathway by interacting with LATS2 and inhibiting its kinase activity to

Published OnlineFirst August 3, 2017; DOI: 10.1158/0008-5472.CAN-17-0229

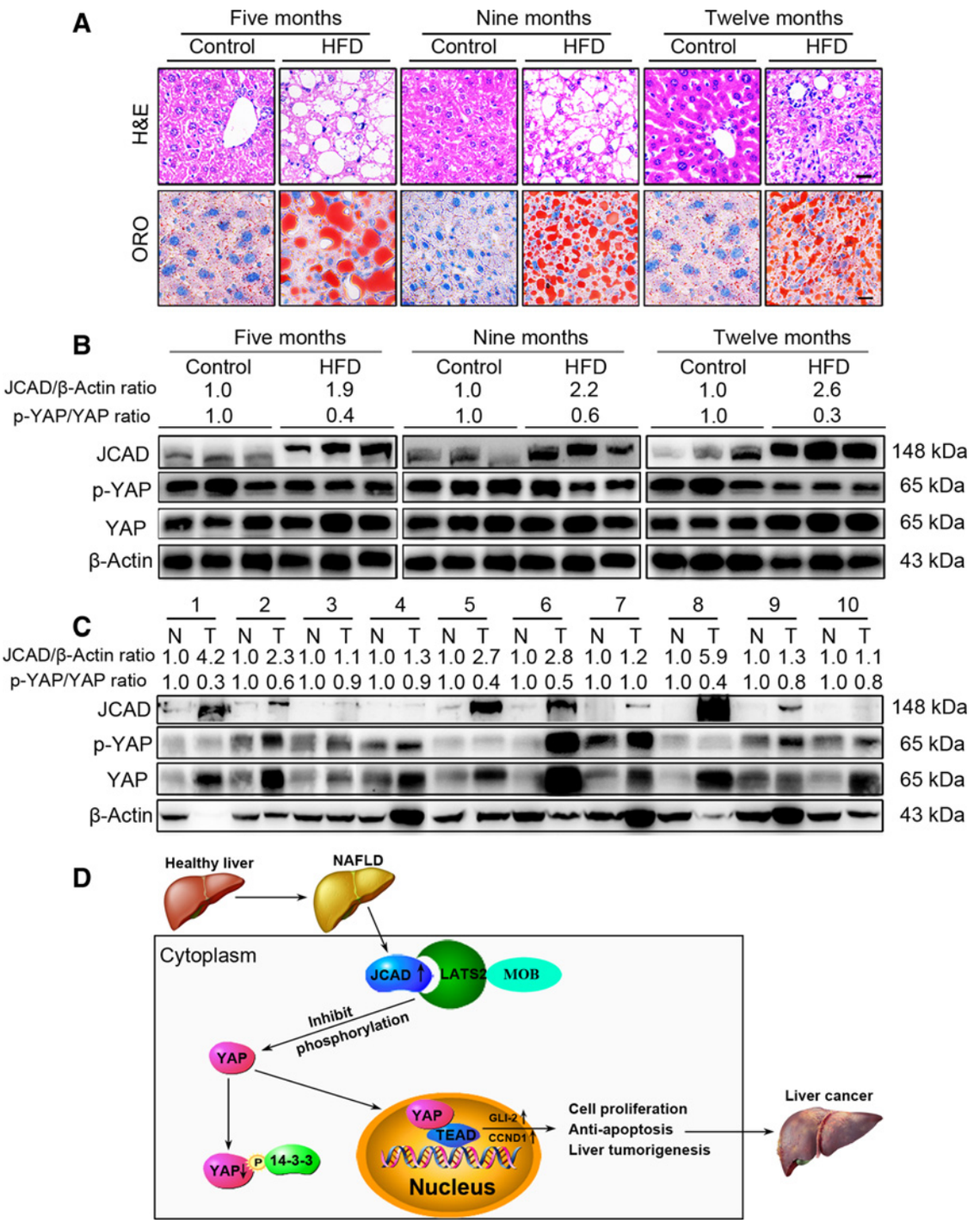

Figure 7.

JCAD was highly expressed in a mouse model of NASH-precarcinoma lesions and human NASH-HCC specimens. **A,** Representative images of hematoxylin and eosin (H&E) and Oil Red O staining of mouse NASH-precarcinoma liver tissues collected after 5, 9, and 12 months of feeding a high-fat diet plus high glucose/fructose in drinking water (magnification, × 40). Scale bars, 10 μm. **B,** Western blot analysis of JCAD protein levels in different stages of mouse liver tissues ($n = 3$ per group). The ratios of JCAD over β-actin and p-Yap over Yap are shown, with the control set to 1.0. **C,** Western blot analysis of JCAD in NASH-HCC and pericarcinoma specimens ($n = 10$ per group). The ratios of JCAD over β-actin and p-YAP over YAP are shown, with the control set to 1.0. **D,** A schematic illustration to indicate the involvement of JCAD in the Hippo pathway signaling, which contributes to the transition from NASH to HCC. JCAD acts as an upstream regulator, binds to LATS2, whereas it did not affect the interaction between JCAD and MOB, which normally binds to LATS2. The interaction between JCAD and LATS2 affects the kinase activity of the latter and reduced YAP phosphorylation status. Dephosphorylation of YAP leads to its nuclear translocation and binds to TEAD to activate the downstream genes (such as *CCND1* and *GLI-2*) transcription; meanwhile the phosphorylated YAP binds to 14-3-3 and results in its cytoplasm retention. Consequently, through the Hippo signaling pathway, JCAD contributes to cell proliferation and tumor formation in a steatotic microenvironment.

modulate cell proliferation and morphogenic process. Therefore, JCAD was identified as an oncogenic facilitator that promotes morphogenic and proliferative responses in a steatotic microenvironment. Our findings underscore that JCAD has great potential to indicate the progression of NASH to HCC, and that the Hippo signaling pathway may well be the candidate for intervention by molecular targeting therapeutics.

Disclosure of Potential Conflicts of Interest

No potential conflicts of interest were disclosed.

Authors' Contributions

Conception and design: J. Ye, T.-S. Li, J. Fan, J. Wu
Development of methodology: J. Ye , T.-S. Li, J. Wu
Acquisition of data (provided animals, acquired and managed patients, provided facilities, etc.): J. Ye, T.S. Li, G. Xu, N.-P. Zhang
Analysis and interpretation of data (e.g., statistical analysis, biostatistics, computational analysis): J. Ye, T.S. Li, J. Wu
Writing, review, and/or revision of the manuscript: J. Ye, T.-S. Li, J. Wu
Administrative, technical, or material support (i.e., reporting or organizing data, constructing databases): J. Ye, T.-S. Li, Y.-M. Zhao, J. Wu
Study supervision: J. Fan, J. Wu
Other (financial support and final proving the manuscript): J. Fan, J. Wu

Acknowledgments

The authors are grateful to Shi-Bin Hu, Yu-Feng Yu, and Ke Qiao (Fudan University School of Basic Medical Sciences) for kind technical assistance in lentiviral package, coimmunoprecipitation, and confocal microscopy.

Grant Support

This project was supported by the National Natural Science Foundation and the Ministry of Science and Technology of China (81272436, 81572356, 2016YFE0107400 to J. Wu) and 81272725 and 81530077 to J. Fan.

The costs of publication of this article were defrayed in part by the payment of page charges. This article must therefore be hereby marked *advertisement* in accordance with 18 U.S.C. Section 1734 solely to indicate this fact.

Received January 24, 2017; revised May 31, 2017; accepted July 28, 2017; published OnlineFirst August 3, 2017.

References

1. Wu J. Utilization of animal models to investigate nonalcoholic steatohepatitis-associated hepatocellular carcinoma. Oncotarget 2016;7:42762–76.
2. Asgharpour A, Cazanave SC, Pacana T, Seneshaw M, Vincent R, Banini BA, et al. A diet-induced animal model of non-alcoholic fatty liver disease and hepatocellular cancer. J Hepatol 2016;65:579–88.
3. Sherif ZA, Saeed A, Ghavimi S, Nouraie SM, Laiyemo AO, Brim H, et al. Global epidemiology of nonalcoholic fatty Liver Disease and Perspectives on US Minority Populations. Dig Dis Sci 2016;61:1214–25.
4. Wong RJ, Aguilar M, Cheung R, Perumpail RB, Harrison SA, Younossi ZM, et al. Nonalcoholic steatohepatitis is the second leading etiology of liver disease among adults awaiting liver transplantation in the United States. Gastroenterology 2015;148:547–55.
5. Lazo M, Hernaez R, Eberhardt MS, Bonekamp S, Kamel I, Guallar E, et al. Prevalence of nonalcoholic fatty liver disease in the United States: the third national health and nutrition examination survey, 1988–1994. Am J Epidemiol 2013;178:38–45.
6. Michelotti GA, Machado MV, Diehl AM. NAFLD, NASH and liver cancer. Nat Rev Gastroenterol Hepatol 2013;10:656–65.
7. Zoller H, Tilg H. Nonalcoholic fatty liver disease and hepatocellular carcinoma. Metabolism 2016;65:1151–60.
8. Wolf MJ, Adili A, Piotrowitz K, Abdullah Z, Boege Y, Stemmer K, et al. Metabolic activation of intrahepatic CD8+ T cells and NKT cells causes nonalcoholic steatohepatitis and liver cancer via cross-talk with hepatocytes. Cancer Cell 2014;26:549–64.
9. Gomes AL, Teijeiro A, Buren S, Tummala KS, Yilmaz M, Waisman A, et al. Metabolic inflammation-associated IL-17A causes non-alcoholic steatohepatitis and hepatocellular carcinoma. Cancer Cell 2016;30:161–75.
10. Yoshimoto S, Loo TM, Atarashi K, Kanda H, Sato S, Oyadomari S, et al. Obesity-induced gut microbial metabolite promotes liver cancer through senescence secretome. Nature 2013;499:97–101.
11. Schulze K, Zucman-Rossi J. Translating the molecular diversity of hepatocellular carcinoma into clinical practice. Mol Cell Oncol 2016;3:e1057316.
12. Akashi M, Higashi T, Masuda S, Komori T, Furuse M. A coronary artery disease-associated gene product, JCAD/KIAA1462, is a novel component of endothelial cell-cell junctions. Biochem Biophys Res Commun 2011;413:224–9.
13. Erdmann J, Willenborg C, Nahrstaedt J, Preuss M, Konig IR, Baumert J, et al. Genome-wide association study identifies a new locus for coronary artery disease on chromosome 10p11.23. Eur Heart J 2011;32:158–68.
14. Consortium CADCDG.A genome-wide association study in Europeans and South Asians identifies five new loci for coronary artery disease. Nat Genet 2011;43:339–44.
15. Boyd J, Luo B, Peri S, Wirchansky B, Hughes L, Forsythe C, et al. Whole exome sequence analysis of serous borderline tumors of the ovary. Gynecol Oncol 2013;130:560–4.
16. Fan YH, Ding J, Nguyen S, Liu XJ, Xu G, Zhou HY, et al. Aberrant hedgehog signaling is responsible for the highly invasive behavior of a subpopulation of hepatoma cells. Oncogene 2016;35:116–24.
17. Paramasivam M, Sarkeshik A, Yates JR 3rd,Fernandes MJ, McCollum D. Angiomotin family proteins are novel activators of the LATS2 kinase tumor suppressor. Mol Biol Cell 2011;22:3725–33.
18. Moroishi T, Park HW, Qin B, Chen Q, Meng Z, Plouffe SW, et al. A YAP/TAZ-induced feedback mechanism regulates Hippo pathway homeostasis. Genes Dev 2015;29:1271–84.
19. Pobbati AV, Hong W. Emerging roles of TEAD transcription factors and its coactivators in cancers. Cancer Biol Ther 2013;14:390–8.
20. Guo C, Wang X, Liang L. LATS2-mediated YAP1 phosphorylation is involved in HCC tumorigenesis. Int J Clin Exp Pathol 2015;8:1690–7.
21. Nguyen HB, Babcock JT, Wells CD, Quilliam LA. LKB1 tumor suppressor regulates AMP kinase/mTOR-independent cell growth and proliferation via the phosphorylation of Yap. Oncogene 2013;32:4100–9.
22. Xu G, Ye J, Liu XJ, Zhang NP, Zhao YM, Fan J, et al. Activation of pluripotent genes in hepatic progenitor cells in the transition of non-alcoholic steatohepatitis to pre-malignant lesions. Lab Invest 2017. doi: 10.1038/labinvest.2017.84.
23. El-Serag HB, Lau M, Eschbach K, Davila J, Goodwin J. Epidemiology of hepatocellular carcinoma in Hispanics in the United States. Arch Intern Med 2007;167:1983–9.
24. Rosmorduc O, Fartoux L. HCC and NASH: how strong is the clinical demonstration? Clin Res Hepatol Gastroenterol 2012;36:202–8.
25. Marengo A, Rosso C, Bugianesi E. Liver cancer: connections with obesity, fatty liver, and cirrhosis. Annu Rev Med 2016;67:103–17.
26. Oda K, Uto H, Mawatari S, Ido A. Clinical features of hepatocellular carcinoma associated with nonalcoholic fatty liver disease: a review of human studies. Clin J Gastroenterol 2015;8:1–9.
27. Yu FX, Guan KL. The Hippo pathway: regulators and regulations. Genes Dev 2013;27:355–71.
28. Murakami H, Mizuno T, Taniguchi T, Fujii M, Ishiguro F, Fukui T, et al. LATS2 is a tumor suppressor gene of malignant mesothelioma. Cancer Res 2011;71:873–83.
29. Zhang Y, Hu CF, Chen J, Yan LX, Zeng YX, Shao JY. LATS2 is de-methylated and overexpressed in nasopharyngeal carcinoma and predicts poor prognosis. BMC Cancer 2010;10:538.
30. Xia Y, Gao Y. MicroRNA-181b promotes ovarian cancer cell growth and invasion by targeting LATS2. Biochem Biophys Res Commun 2014;447:446–51.
31. Pan D. The hippo signaling pathway in development and cancer. Dev Cell 2010;19:491–505.

Published OnlineFirst August 3, 2017; DOI: 10.1158/0008-5472.CAN-17-0229

32. Dong J, Feldmann G, Huang J, Wu S, Zhang N, Comerford SA, et al. Elucidation of a universal size-control mechanism in *Drosophila* and mammals. Cell 2007;130:1120–33.
33. Chen X, Lingala S, Khoobyari S, Nolta J, Zern MA, Wu J. Epithelial mesenchymal transition and hedgehog signaling activation are associated with chemoresistance and invasion of hepatoma subpopulations. J Hepatol 2011;55:838–45.
34. Ding J, Zhou XT, Zou HY, Wu J. Hedgehog signaling pathway affects the sensitivity of hepatoma cells to drug therapy through the ABCC1 transporter. Lab Invest 2017;97:819–32.
35. Hager J, Dina C, Francke S, Dubois S, Houari M, Vatin V, et al. A genome-wide scan for human obesity genes reveals a major susceptibility locus on chromosome 10. Nat Genet 1998;20:304–8.
36. Hinney A, Ziegler A, Oeffner F, Wedewardt C, Vogel M, Wulftange H, et al. Independent confirmation of a major locus for obesity on chromosome 10. J Clin Endocrinol Metab 2000;85:2962–5.
37. Price RA, Li WD, Bernstein A, Crystal A, Golding EM, Weisberg SJ, et al. A locus affecting obesity in human chromosome region 10p12. Diabetologia 2001;44:363–6.

Published OnlineFirst August 3, 2017; DOI: 10.1158/0008-5472.CAN-17-0229

Cancer Research
The Journal of Cancer Research (1916–1930) | The American Journal of Cancer (1931–1940)

AACR American Association for Cancer Research

JCAD Promotes Progression of Nonalcoholic Steatohepatitis to Liver Cancer by Inhibiting LATS2 Kinase Activity

Juan Ye, Tian-Sheng Li, Gang Xu, et al.

Cancer Res 2017;77:5287-5300. Published OnlineFirst August 3, 2017.